A triple-combination nanotechnology platform based on multifunctional RNA hydrogel for lung cancer therapy

Junwei Li[1,2], Dandan Yuan[1,2], Xiangjiang Zheng[1], Xinyue Zhang[1],
Xuemei Li[1*] & Shusheng Zhang[1*]

[1]*Collaborative Innovation Center of Tumor Marker Detection Technology, Equipment and Diagnosis-Therapy Integration in Universities of Shandong, Shandong Province Key Laboratory of Detection Technology for Tumor Makers, School of Chemistry and Chemical Engineering, Linyi University, Linyi 276005, China;*
[2]*College of Chemistry, Chemical Engineering and Materials Science, Cooperative Innovation Center of Functionalized Probes for Chemical Imaging in Universities of Shandong, Shandong Normal University, Jinan 250014, China*

Conventional cancer combination therapy usually involves systemic delivery of anticancer drugs which may lead to the destruction of normal cells and physiological toxicity due to the lack of targeting ability and toxicity of drug carriers. In the present study, a triple combination nanosystem of gene therapy, chemotherapy and phototherapy delivered by multifunctional RNA nanohydrogels (RNA NHs) was established. By taking the advantages of DNA nanotechnology and rolling circle transcription (RCT), three lung cancer inhibitor microRNA (let-7a, microRNA 34a, microRNA 145) hairpins were integrated in one RNA NH nanoparticle, leading to the simultaneous silencing of three targeted mRNAs. Meanwhile, RNA NH carried doxorubicin (DOX, a chemotherapy drug) as well as 5,10,15,20-tetrakis (1-methylpyridinium-4-yl) porphyrin (TMPyP4, a photosensitizer) and delivered these drugs to cancer cells. It was demonstrated that lung cancer inhibitor microRNAs integrated in RNA NHs, DOX and TMPyP4 could play a synergistic anti-cancer role in multi-drug resistance cancer cells. Under the action of aptamer sequence S6 that was modified with cholesterol, the resulting RNA NHs were condensed to feasible size without the assistance of polyelectrolyte condensation reagents and showed cancer-specific cellular targeting. Subsequently, thousands of copies of miRNA together with chemotherapy drug as well as photosensitizer were delivered to cancer cells specifically, and an ideal synergistic treatment effect was achieved *in vivo*, thus playing a combined role of gene therapy, chemotherapy and phototherapy. Through this study, it can be concluded that the triple combination therapy nanosystem can overcome the multi-drug resistance caused by the malfunction of genes in chemotherapy and shows a great potential in the field of multifunctional synergistic cancer treatment.

RNA nanohydrogel, phototherapy, drug delivery, gene therapy, lung cancer

1 Introduction

Cancer is a leading cause of death in China and it is also a major public health problem. In 2015, more than 4 million new cancer cases and 2.8 million cancer deaths were reported in China [1,2] in which lung cancer is one of the most common cancers and the main cause of death for cancer patients. In developed countries, it has surpassed breast cancer as the main cause of cancer deaths in females cancer patients [3,4]. Therefore, it is a task of top priority for clinicians and scientists all over the world to develop effective therapeutic methods for lung cancer treatment. Chemother-

---

*Corresponding authors (email: xuemei_li@yeah.net; shushzhang@126.com)

apy, a primary method for cancer therapy, generally uses small molecular anticancer drugs to improve the therapeutic effects in clinic. However, there are still serious deficiencies in conventional chemotherapy, such as serious adverse reactions and multidrug resistance [5–7]. RNA interference (RNAi) technique, an endogenous pathway that induces gene silencing effects at a post-translational level by directly blocking the translation of their target messenger RNAs (mRNAs) or by inhibiting protein production via mRNA destabilization controlled by microRNAs (miRNAs), has served as a promising diagnostic and therapeutic tools of lung cancer [8–11]. Moreover, miRNA-based therapy can increase the sensitization of cancer cells to conventional chemotherapeutic drugs by down-regulating the expression of transporters, silencing anti-apoptotic genes, suppressing tumor angiogenesis and promoting cell apoptosis [12–15]. Therefore, the combination of chemotherapeutic agents and therapeutic miRNA for cancer treatment has become a promising anticancer strategy to improve the therapeutic efficacy, reduce side effects and overcome drug resistance [16–22]. In addition, chemotherapy resistance is a challenge to effective treatment of cancer, which is usually affected by multiple gene pathways that are highly interdependent. According to these gene pathways, the mechanisms of chemoresistance on most multidrug-resistant (MDR) cancers are classified into efflux pump and non-efflux pump resistance [23–25]. To alleviate the problem of chemoresistance, the simultaneous co-delivery of different types of miRNAs might be required for the combination therapy to realize gene silencing for both pump and non-pump resistance at the same time. However, there are still remain many problems in delivering miRNAs to tumors, including the low loading efficacy for siRNA cargo, instability of bloodstream and poor targeting ability. To further expand the versatility of these multiple types of miRNAs in the therapeutic applications, the next goal is to develop an all-in-one miRNA delivery system that can simultaneously delivers three types of miRNAs for potent synergistic therapies based on RNAi.

DNA or RNA materials have shown unprecedented applications potential in the delivery of drug [26–28]. Rolling circle transcription (RCT), is an efficient tool for synthesizing microRNA while taking its small circular DNA as the template, and particularly when designed rationally, the polymerized RNAs self-assembles into the microsponges with the diameter of 2 mm [29,30]. The RNA nanohydrogels with controllable size for increasing the loading efficiency of miRNA can be synthesized through self-assembly without the aid of polycationic agents. In the present study, a new triple combination therapy nanosystem based on the RNA nanohydrogels containing the copies of three microRNAs (hairpins let-7a, microRNA 34a (miR-34a) and microRNA 145 (miR-145)) acting as lung cancer inhibitors was developed. Let-7a inhibits the expression of oncogenes involved

in cell proliferation, such as MYC, RAS, HMGA2, additionally, let-7a regulates the cell cycle by inhibiting CDK6 expression [31,32]. It has been demonstrated that miR-34a can improve the anti-tumor activity by inhibiting the expression of an anti-apoptosis gene, Bcl-2 [33–35]. MiR-145 inhibits non-small cell lung cancer (NSCLC) cell proliferation partly by mediating the regulation of c-myc/eIF4E pathway, and then further controls cell cycle by CDK4 regulation [36–38]. In this study, the RNA nanohydrogels as carriers of concurrently possessing gene regulatory effect were synthesized successfully via DNA nanotechnology and RCT. Moreover, a triple therapy system based on RNA hydrogels was constructed by co-loading the photosensitizer TMPyP4 and the anticancer drug DOX. The introduction of aptamer sequence S6 achieved highly specific recognition and effective delivery. The RNA hydrogel nanoparticles combined with TMPyP4 and DOX significantly improved drug release efficiency and achieved the gene-chemotherapy-photothermal treatment (PPT) three-in-one combination at the same time, thereby greatly increasing the mortality rate of cancer cells. According to the results of this study, it can be concluded that the smart triple combination therapy nanosystem possesses a great potential in the field of multifunctional synergistic cancer treatment.

2 Experimental

2.1 Reagents

All oligonucleotides used in the study were purchased from Takara Biotechnology Co., Ltd. (China), and the sequences are provided in Table S1 (Supporting Information online). DOX was obtained from Sangon Biotech Co., Ltd. (China). 2,7-Dichlorofluorescin diacetate (DCFH-DA) and 5,10,15,20-tetrakis(1-methylpyridinium 4-yl) porphyrin (TMPyP4) were obtained from Sigma-Aldrich (USA). T7 RNA polymerase and ribonucleotide mixture were purchased from New England Biolabs. T4 DNA ligase was purchased from Thermo Scientific (USA). Cell lines (A549 cell, HeLa cell and L02 cell) were purchased from the Boster Biological Technology Co., Ltd. (China). Dul-becco's modfied eagle medium (DMEM) was obtained from Hy-Clone. $MgCl_2$, Tris-HCl, Glucose were acquired from Aladdin (China). The cell counting kit-8 (CCK-8) was purchased from KangLang Biotechnology Co., Ltd. (China). All other chemicals were of analytical grade and used as received without further purification.

2.2 Apparatus

Confocal fluorescence imaging was performed by a Leica TCS SP8 inverted confocal microscope (Leica SP8). Absorption spectra were determined by UV-Vis spectro-

photometer (NanoDrop 2000, Thermo Scientific). The transmission electron microscopy (TEM) images were acquired using a TEM instrument (JEM-2100, Hitachi, Japan). Zeta potential measurement was performed at 25 °C on a Zeta-size Nano instrument (Zen 3600, Malvern Instruments Ltd.). Fluorescence spectra were measured by a fluorescence spectrophotometer (F-4600, Hitachi). The vivo imaging was performed by an IVIS vivo imaging system.

2.3 Synthesis of RNA transcripts and RNA transcriptions/FAM-S6APT-CHOL (RNA nano-hydrogels, RNA NHs) complexes

All sequences were dissolved and diluted in nuclease-free water. To synthesize circular DNA, the Asm-DNA and the three DNA templates were mixed, and the mixture solution was denatured at 95 °C for 2 min and then slowly cooled down to 25 °C, yielding circular DNA/T7 promoter hybrids with the nick. Then, T4 ligase was added and the mixture was incubated for 12 h at 16 °C. Next, the mixture was mixed with T7 RNA polymerase (5 U/μL) in the reaction buffer (4 mM Tris-HCl (pH 7.9), 10 mM $MgCl_2$, 1 mM DTT and 0.2 mM spermidine) containing 2 mM rNTP (ribonucleotide solution mix, NEB) and 1 U/μL RNase inhibitor in the final concentration; the total reaction volume was 50 mL. Consequently, the mixture was incubated at 37 °C for 1.5 h to generate the polymerized RNA transcripts (RNA transcriptions). Finally, to generate the condensed RNA nanohydrogels, we added FAM-S6apt-CHOL fragments to base-paired RNA transcripts (RNA transcriptions) dissolved in 30 mM Tris-HCl (pH 7.8) buffer including 10 mM $MgCl_2$. The resulting mixture was subjected to heat denaturation at 65 °C for 5 min, and subsequently, cooled down to 4 °C for base pairing between RNA transcriptions and FAM-S6apt-CHOL.

The single RNA nanohydrogels were obtained by mixing single RNA transcriptions with the FAM-S6apt-CHOL hybrids at the same conditions.

2.4 UV-Vis absorption and fluorescence measurement

TMPyP4 was diluted to 25 μM. Then different volumes (0, 1, 2, 3, 4, 5, 10 and 20 μL) of RNA NHs were added to the TMPyP4 solution. The mixture was incubated at 37 °C for 2 h to generate the RNA NHs-T. In the same way, different volumes (0, 5, 10, 40, 60, and 80 μL) of RNA NHs were added into 100 μL of DOX (20 μM) to incubated at 37 °C for 2 h. Following 2 h incubation, the mixture was subjected to two centrifuge wash cycles (10,000 r/min, 20 min) to remove excess drug and resuspended in 1% bovine serum albumin (BSA) containing washing buffer (4.5 g/L glucose and 5 mM $MgCl_2$ in Dulbecco's PBS with calcium chloride and magnesium chloride (Sigma-Aldrich)). To study the interaction

between RNA NHs and TMPyP4, the absorption at 422 nm was detected by a UV-NanoDrop 2000 spectrophotometer. The fluorescence spectra of DOX after incubation with RNA NHs (RNA NHs-D) were measured by a FL-4600 fluorescence spectrometer.

2.5 *In vitro* stability test of RNA NHs under serum condition

For the stability studies of RNA transcripts or RNA NHs against serum nucleases, fetal bovine serum (FBS) was mixed with RNA transcripts or RNA NHs at the final concentration of 30% and then incubate at 37 °C during the indicated time period. Each sample was analyzed on the 15% non-denaturing polyacrylamide gel (15%) under TBE buffer.

2.6 Cell culture

A549 cells, HeLa cells and L02 cells were maintained in DMEM cell medium (penicillin, 100 U/mL; streptomycin, 100 μg/mL; and Hyclone) supplemented with 10% FBS and maintained at 37 °C in a humidified atmosphere with 5% CO_2.

2.7 Fluoresence imaging

Cancer cells were seeded in a 35 mm confocal dish and allowed to further grow for 12 h before the experiments. Cells (10^6 cells/mL) were incubated with RNA NHs or RNA NHs-D complexes for 2 h at 37 °C, followed by washing with 1 mL of phosphate buffer (pH 7.4) twice and suspended in 200 μL of DMEM medium before imaging. Nuclei were visualized after staining with 4′,6′-diamidino-2-phenylindole (DAPI) for 5 min. All the wide-field or confocal laser scanning microscopy (CLSM) images were collected on the Leica TCS SP5 II microscopy, with the following excitation wavelengths and emission filters: DOX, 488 nm laser line excitation, emission BP (580±20) nm filter; fluorescein 5-isothiocyanate (FITC), 488 nm laser line excitation, emission BP (520±20) nm filter. After confocal imaging analysis, the samples were analyzed using a CutoFLEX flow cytometer. The single-RNA NHs were detected in the same method.

2.8 Intracellular reactive oxygen species generation and drug release

A549 cells were seeded in 35 mm plastic-bottomed dishes and grown for 12 h. The culture medium was replaced with complete culture medium containing RNA NHs, RNA NHs-T, respectively. And then, the cells were washed twice in washing buffer (1% BSA). 50 μM DCFH-DA (Molecular Probes) was added in prepared serum-free DMEM medium

to the cells for 40 min at 37 °C. Subsequently, the cells were irradiated for 50 min (650 nm, 12 mW/cm^2). Finally, cells were resuspended in 1 mL Dulbecco's phosphate buffered saline (DPBS) for flow cytometry analysis.

To observe intracellular DOX release based on ROS generation, A549 cells were incubated with RNA NHs-D-T for 2 h at 37 °C, followed by treating with DCFH-DA. Then, the cells were irradiated with or without 650 nm light for 50 min. The triggered drug release process was further observed by confocal laser scanning microscopy imaging.

2.9   Cell viability studies

The cytotoxicity of free DOX, TMPyP4, RNA NHs-D, RNA NHs-T or RNA NHs-D-T complexes for each individual type of cell were determined by the Cell Counting Kit-8 (CCK-8) assay (KaLang Co., Ltd., China). Cells were seeded into a 96-well plate at a density of 1×10^4 cells per well and cultured for 12 h followed by treating with the materials mentioned at 37 °C for different time. And then, the supernatant was removed and replaced by 100 μL fresh cell culture medium for further cell growth and incubated for 24 h. Then, 10 μL of CCK-8 solution was added to each well and incubated for 1 h. The absorbance at 450 nm of formazan was recorded by using a microplate reader.

2.10   *In vivo* studies

All animal study was conducted according to national guidelines and with approval of the regional ethics committee for animal experiments. The lung cancer model was established by subcutaneously injecting A549 cells into BALB/c naked mice. When the tumor size reached approximately 100 mm^3, the tumor-bearing mice were randomly divided into two groups: (a) injected with PBS; (b) injected with RNA NHs-D-T and irradiated by 650 nm light (12 mW/cm^2, after injection). *In vivo* fluorescence imaging was conducted using an IVIS vivo imaging system. The tumor sizes were recorded every 3 days, with their lengths and widths measured by a digital caliper. The tumor volume was calculated according to the following formula: width$^2\times$length/2.

3   Results and discussion

3.1   Synthesis of RNA transcriptions and RNA nano-hydrogels (RNA NHs)

The Y-shaped monomer serving as a building unit was assembled from three single-stranded DNAs (ssDNAs), and each strand has a "sticky end" fragment used to hybridize with its complementary DNA. Three kinds of linear ssDNA template were designed to be complementary to T7 promoter

primer, FAM-S6 apt-CHOL, antisense sequence of let-7a, miR-34a and miR-145, respectively.

The gel electrophoresis results of antisense-red fluorescent protein (RFP) siRNA, antisense anti-RFP siRNA, DNA-Chol conjugate and FA-DNA conjugate are shown in Figure 1 and Table S1, respectively. First of all, the designed linear DNA template was transcribed into RNA transcripts via RCT reaction (Scheme 1(a) and Table S1). The ends of the Asm-DNA have T7 promoter sequences. Subsequently, the linear DNA template was annealed with T7 primers using the complementary sequences and the nicked sequences were connected by T4 DNA ligase. The closed circular DNA was then used to produce RNA transcripts via RCT, encoding both antisense and sense sequences of microRNA and yielding hairpin RNA structures. Next, RNA transcriptions/FAM-S6apt-CHOL complexes (RNA NHs) were generated with the base-paired RNA transcriptions with FAM-S6 apt-CHOL fragments. The advanced design of microRNA delivery in this study is that three types of microRNA molecules can be easily assembled into RNA NHs, thus achieving the increase of cargo loading. Therefore, a multifunctional drug delivery nanosystem that has possesses the ability of combining chemotherapy and phototherapy was finally constructed. Based on the advanced design, the RNA NHs can provide the binding sites for the loading of TMPyP4,
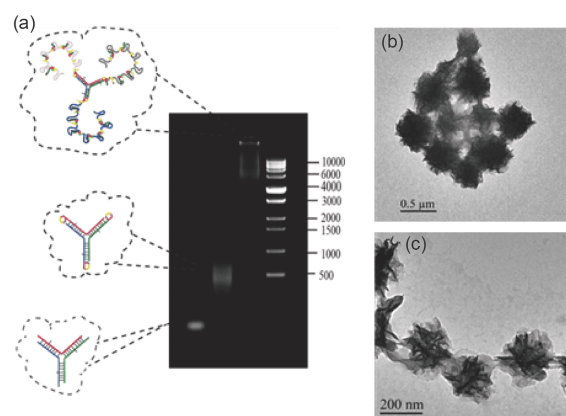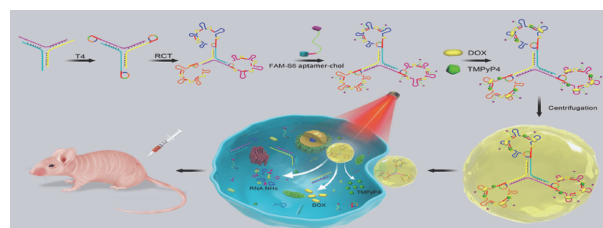

Figure 1   (a) Illustration of the formation of RNA NHs bygel electrophoresis. Images of the size (b) and shape (c) of RNA NHs under transmission electron microscopy (color online).

Scheme 1   Schematic illustration of the self-assembly and mechanism of RNA NHs-D-T (color online).

which can insert into G-quadruplex as well as DOX. Meanwhile, G-quadruplex and DOX can preferentially bind to double-stranded GC or CG sequences [39,40]. Once endocytosis occurs, DOX can be released and the reactive oxygen species (ROS) induced by TMPyP4 molecules were generated inside the living cells under light irradiation. Therefore, the therapeutic effect of RNA NHs-DOX-TMPyP4 (RNA NHs-D-T) on the target cells is superior to the RNA NHs treatment. In addition, the single-RNA NHs only containing one kind of microRNA was synthesized in the same ways (Scheme 1(b)).

3.2 Characterization of RNA NHs

As shown in Figure 1(a), the synthetic sequences were analyzed through gel electrophoresis, and the results indicated the successful formation of RNA NHs via RCT. In addition, it was shown in Figure 1(b) that the diameter of the RNA transcript producing without the help of cholesterol is about 0.5 µM. TEM images showed the morphology of the RNA NHs and their average size is approximately 160 nm (Figure 1(c)). The RNA transcriptions had the micro-sized hydrodynamic diameter, while their particle sizes were further significantly reduced to about 160 nm after the hybridization of RNA transcripts with FAM-S6apt-CHOL (Figure S1, Supporting Information online). The reason for this phenomenon is that cholesterol has the property that of making the structure of the RNA NHs more compact caused by hydrophobic interaction [41,42]. After the assembling of RNA NHs, the zeta potential changed to −8.29 mV (Figure S2). The zeta potential measurement also showed that the negative surface charge of RNA NHs was moderately weaker than that of RNA transcriptions.

Furthermore, the single-RNA NHs was also characterized through gel electrophoresis, and the results indicated the successful production of single-RNA NHs through RCT (Figure S3). The zeta potential of the three types of single-RNA NHs (let 7a, miR 34a, miR 145) changed accordingly, which showed the reduction of hydrogel surface charge (Figure S4). The morphologies of the RNA superstructures that treated with or without FAM-S6apt-CHOL were detected by TEM after 1.5 h of RCT reaction (Figure S5). The size reduction of the single-RNA NHs indicated that the RNA transcripts were condensed into highly packed particles due to the acquired amphiphilicity.

3.3 Improvement of the stability of RNA NHs in serum

How to enhance the stability of RNA NHs against the nuclease attack in bloodstream is a major challenge for systemic delivery of microRNA. The efficacy of RNA transcriptions and RNA NHs in serum was further examined by 15% non-denaturing polyacrylamide gel electrophoresis

after the treatment with 30% FBS. As shown in Figure S6, RNA transcriptions were obviously degraded after 6 h incubation, whereas RNA NHs were more resistant to nuclease attack and about 80% of RNA NHs still remained unchanged even after 6 h of incubation. These results indicated that RNA NHs are much more stable than RNA transcriptions in serum, which was attributed to the compacted structure of the RNA NHs. Therefore, the stability of RNA NHs in serum can be enhanced after the treatment with FAM-S6apt-CHOL.

3.4 Specific binding and internalization of RNA NHs

To confirm whether the RNA NHs can effectively target and internalize the tumor cells, the cellular uptake of RNA NHs in A549 cells, HeLa cells (human cervix adenocarcinoma cell) and L02 cells (human hepatocyte cell) was evaluated by confocal microscopy observation and flow cytometry analysis. The above three kinds of cell were incubated with RNA NHs at 37 °C for 2 h, respectively. Figure 2(a) shows that after the incubation, the green fluorescent intensity in the cytoplasm of A549 cells was much higher than that in the cytoplasm of HeLa cells and L02 cells. These results suggest that once these hydrogel nanoparticles were equipped with the aptamers, more effective cellular uptake can be achieved. At the same time, these results were also verified through flow cytometry analysis (Figure 2(b)). The significant difference of the fluorescence signal between A549 cells and HeLa cells or L02 cells can also provide a tool for cancer discrimination. The representative fluorescence images also demonstrated the successful internalization of these nanoparticles in A549 cells.

Furthermore, the internalization of single-RNA NHs into A549 cell was verified by confocal microscopic image. As presented in Figure S7, the let 7a, miR 34a and miR 145 single-RNA NHs as well the mixture of them had different degree of endocytosis, which further demonstrated the specific recognition of target A549 cells by RNA NHs caused by existence of S6 aptamer [43]. Meanwhile, the cells were treated with DAPI and RNA NHs-D to explore the colocalization of RNA NHs. The images show that the DOX loaded on the RNA NHs was successfully conveyed into cell cytoplasm (Figure S8).

3.5 Preparation of drug/TMPyP4-loaded RNA NHs and synergetic drug release

In this design of the present study, the G-quadruplex and the double-strand DNA sequence provides the binding sites for TMPyP4 and DOX, respectively. Therefore, this nanosystem based on the RNA NHs can achieve an enhanced synergistic therapy effect by specific recognition of A549 cells. To study the loading efficiency of TMPyP4, the TMPyP4-loading capacity was quantified with UV-Vis spectra analysis, and
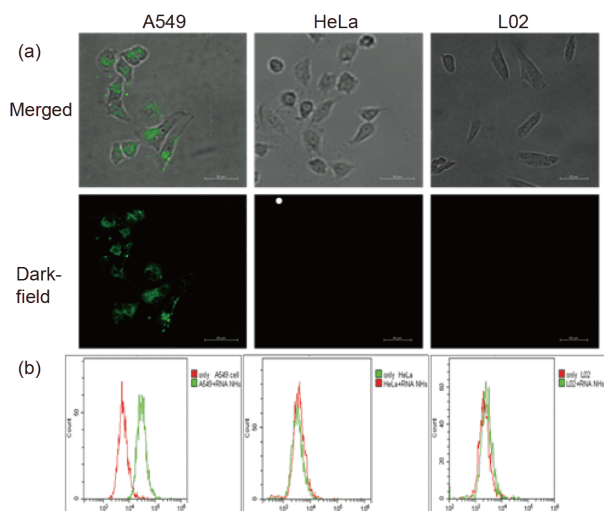
Figure 2   (a) CLSM images of A549 cells, HeLa cells and L02 cells after incubation with RNA NHs at 37 °C for 2 h. (b) Flow cytometric assay of A549 cells, HeLa cells and L02 cells incubated with or without RNA NHs (color online).

Figure 3   (a) UV-Vis absorption spectra of TMPyP4 with RNA NHs ranged from 0 to 20 µL. (b) Fluorescence absorption spectra of DOX solution with the increase of RNA NHs addition (ranged from 0 to 80 µL). (c) CLSM images of A549 cells incubated with RNA NHs and DAPI with or without 650 nm laser irradiation (color online).

the absorption curve of the RNA NHs with different volume ranging from 0 to 20 µL was plotted in the presence of 5 µL TMPyP4 (25 µM). With the addition of the RNA NHs, the absorbance of TMPyP4 at the wavelength of 422 nm was decreased, and the peak position was red-shifted to 435 nm (Figure 3(a)). Thus, in the presence of 5 µL TMPyP4 with the concentration of 25 µM, the optimal volume of RNA NHs was estimated to be 20 µL according to the spectral shifts. Similarly, the fluorescence spectra of DOX (20 µM, 100 µL) incubated with different volume of RNA NHs ranging from 0 to 80 µL were detected (Figure 3(b)). The fluorescence intensity of DOX could reach the relatively low point when the volume of RNA NHs reached 80 µL, indicating the relative saturated binding between DOX and RNA NHs.

To validate the mechanism of the therapeutic synergism elicited by the combination of TMPyP4 and DOX in A549 cells, the A549 cells were incubated with RNA NHs-D-T and then treated with or without laser irradiation (Figure 3(c)). After the incubation, the fluorescence of DOX around the nucleus was primarily detected. Subsequently, after laser irradiation, the merged image of the red fluorescence (from DOX) and the blue fluorescence (from DAPI) were detected at the nucleus, which showed that DOX had internalized the cell nucleus. These results clearly demonstrated that the nanosystem has good photocontrollable drug release capability.

3.6   Study of intracellular ROS formation

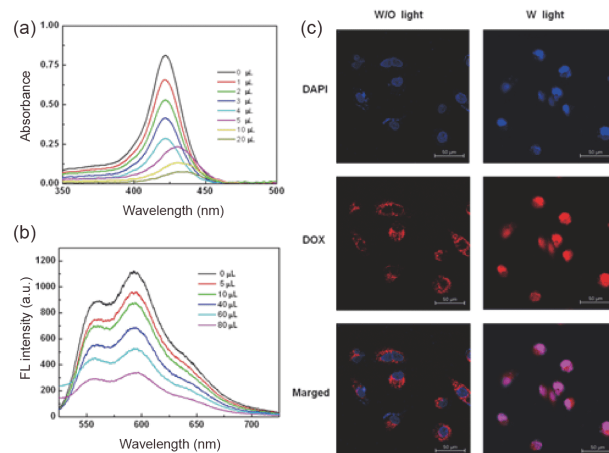TMPyP4, a photosensitizer, has the ability to generate amounts of ROS under the condition of laser irradiation. To illustrate for the effectiveness of RNA NHs-T, the intracellular ROS formation was investigated. DCFH-DA (2′,7′-dichlorodihydrofluorescein diacetate), which is used as a singlet oxygen probe, was added in A549 cells culture during the combined process. The experimental results showed a more obvious fluorescence change in the cells treated with RNA NHs-T, compared with that treated with RNA NHs and that were not treated (Figure S9). Moreover, the results further proved the existence of intracellular ROS. The accumulation of intracellular ROS induced by RNA NHs-T can cause cell death following exposure to the irradiation.

3.7   Cytotoxicity assay and *in vivo* tumor effect

The *in vitro* cytotoxicity of RNA NHs on A549 cells was evaluated by CCK-8 assay. In addition, *in vitro* experiments were performed to determine the cytotoxicity of single RNA NHs on A549 cells at different times, and the RNA nanohydrogel with a template containing no microRNA complementary sequence was composited as a negative control. As shown in Figure 4(a), the viability of A549 cells treated with the negative control was higher than 80%.

The cells treated with single-RNA NHs displayed a reduced viability. Although single miRNA can inhibit cell proliferation, it cannot induce strong cytotoxicity completely. After the incubation of A549 cells with RNA NHs-D, RNA NHs-T, RNA NHs-D-T, respectively, it was revealed that compared with RNA NHs-D-T without the laser irradiation, the combination therapy (RNA NHs-D-T with the irradiation under the wavelength of 650 nm) induced considerably obvious inhibition of cell proliferation. The viability of the cells treated with RNA NHs-D-T was as low as 30% after 72 h, whereas in the cells treated with RNA NHs-D
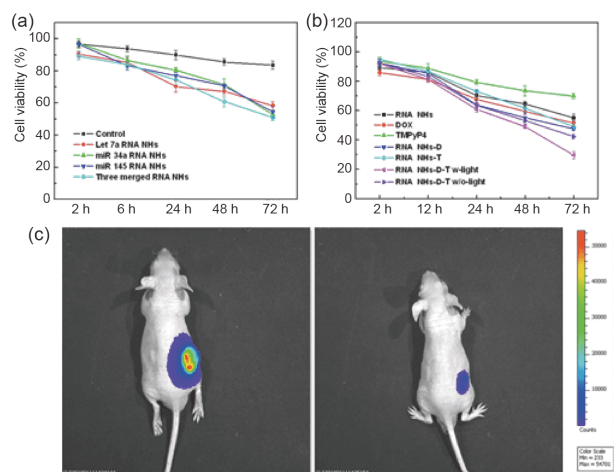
Figure 4 (a) Viability assays of A549 cells that were treated with single-RNA NHs. (b) Viability assays of A549 cells that were treated with free DOX, free TMPyP4, RNA NHs, RNA NHs-D, RNA NHs-T, RNA NHs-D-T, respectively. (c) *In vivo* fluorescence images of A549 tumor-bearing mouse treated with PBS (left) and RNA NHs-D-T (right) (color online).

and RNA NHs-T, the inhibition of cell proliferation was slightly reduced under the same conditions. The results suggest the synergistic cytotoxicity caused by co-delivery of DOX and miRNAs. Compared with the experimental group of RNA NHs-D-T in the absence of laser irradiation and other controlled trials, the combination therapy could induce considerably obvious inhibition of cell proliferation, and the therapeutic efficacy of RNA NHs-D-T was the most remarkable. In addition, the viability of HeLa cells (Figure S10 (a)) and L02 cells (Figure S10(b)) was slightly affected by treating with all materials containing the aptamers that can specifically target A549 cells.

The *in vivo* pharmacokinetic and therapeutic profile of the RNA nanohydrogel in the subcutaneous A549 lung cancer tissue of the mouse model was further investigated. Hydrogel carriers loaded with DOX and TMPyP4 were implanted in the tissue adjacent to the lung tumor when the volume of tumor reached about ~100 mm^3. The tumor area displayed a strong fluorescence signal and the high contrast of tumor imaging could be distinguished from the control area (Figure 4(c)). *In vivo* imaging of mice revealed that the macro-metastasis was inexistent in the mice and the delivery capacity of the RNA NHs-D-T *in vivo* was highly efficient. Moreover, RNA NHs-D-T was able to accumulate similarly in tumor tissues and plays a role in inhibiting the proliferation of tumor cells. The mice were then sacrificed and a part of the tumor tissues were collected (Figure S11(a)). Subsequently, *in vivo* treatment effect of RNA NHs-D-T on tumor was assessed by monitoring the change of relative tumor volume (Figure S11(b)). The growth of the tumor tissues obviously slowed down after the tumor bearing mice were treated with RNA NHs-D-T, suggesting that the therapeutic effect in the mice treated with RNA NHs-D-T was better than that in the mice treated with PBS. This result confirmed the effect of this platform on the targeted therapy.

4 Conclusions

In this study, a triple-combination therapy RNA nanosystem based on RNA nanohydrogel containing three types of microRNA was designed for the detection and treatment of lung cancer. The RNA NHs provide a means of rapidly synthesizing diversiform microRNA that enables to realize gene regulation in nanohydrogel. The simultaneous co-delivery of the three types of miRNAs realizes gene silencing for both pump and non-pump resistance of chemotherapy at the same time, thus solving the problem of chemoresistance. Furthermore, the RNA NHs co-loading DOX and TMPyP4 can be delivered into cancer cells efficiently via aptamer, thus resulting in smart drug release. In the presence of lasers, the triple combination therapy nanosystem that combines gene therapy, chemotherapy and photodynamics therapy shows a significant inhibiting effect on the proliferation of the target tumor cells and ideal treatment effect. Therefore, based on these results, this RNA hydrogels platform is expected to provide a new approach for the therapy of lung cancer.

Conflict of interest The authors declare that they have no conflict of interest.

1 Chen W, Zheng R, Baade PD, Zhang S, Zeng H, Bray F, Jemal A, Yu XQ, He J. *CA-A Cancer J Clinicians*, 2016, 66: 115–132

2 Alam SK, Astone M, Liu P, Hall SR, Coyle AM, Dankert EN, Hoffman DK, Zhang W, Kuang R, Roden AC, Mansfield AS, Hoeppner LH. *Commun Biol*, 2018, 1: 43

3 Inamura K. *Cells*, 2017, 6: 12

4 Siegel RL, Miller KD, Fedewa SA, Ahnen DJ, Meester RG, Barzi A, Jemal A. *Ca A Cancer J Clin*, 2017, 67: 104-117

5 Cui H, Huan ML, Ye WL, Liu DZ, Teng ZH, Mei QB, Zhou SY. *Mol Pharm*, 2017, 14: 746–756

6 Chen H, Gu Z, An H, Chen C, Chen J, Cui R, Chen S, Chen W, Chen X, Chen X, Chen Z, Ding B, Dong Q, Fan Q, Fu T, Hou D, Jiang Q, Ke H, Jiang X, Liu G, Li S, Li T, Liu Z, Nie G, Ovais M, Pang D, Qiu N, Shen Y, Tian H, Wang C, Wang H, Wang Z, Xu H, Xu JF, Yang X, Zhu S, Zheng X, Zhang X, Zhao Y, Tan W, Zhang X, Zhao Y. *Sci China Chem*, 2018, 61: 1503–1552

7 Pugazhendhi A, Edison TNJI, Velmurugan BK, Jacob JA. *Karuppusamy I*, 2018, 200: 26

8 Dua K, Hansbro NG, Foster PS, Hansbro PM. *Drug Deliv Transl Res*,

2016, 7: 1-11

9   Wei H, Zhang X, Cheng C, Cheng SX, Zhuo RX. *Biomaterials*, 2007, 28: 99–107

10 Zhang Z, Shi L, Wu C, Su Y, Qian J, Deng H, Zhu X. *ACS Appl Mater Interfaces*, 2017, 9: 29505–29514

11 Li C, Li H, Ge J, Jie G. *Chem Commun*, 2019, 55: 3919–3922

12 Dai X, Tan C. *Adv Drug Deliver Rev*, 2015, 81: 184–197

13 Chen J, Luo H, Liu Y, Zhang W, Li H, Luo T, Zhang K, Zhao Y, Liu J. *ACS Nano*, 2017, 11: 12849–12862

14 Cheng Y, Cheng H, Jiang C, Qiu X, Wang K, Huan W, Yuan A, Wu J, Hu Y. *Nat Commun*, 2015, 6: 8785

15 Sun M, Qian QH, Shi LL, Xu L, Liu QF, Zhou LZ, Zhu XY, Yue JM, Yan DY. *Sci China Chem*, 2019, 62: 1-6

16 Chakraborty C, Sharma AR, Sharma G, Sarkar BK, Lee SS. *Oncotarget*, 2018, 9: 10164–10174

17 Park H, Yang J, Lee J, Haam S, Choi IH, Yoo KH. *ACS Nano*, 2009, 3: 2919–2926

18 Guo F, Yu M, Wang J, Tan F, Li N. *ACS Appl Mater Interfaces*, 2015, 7: 20556–20567

19 Feng L, Gao M, Tao D, Chen Q, Wang H, Dong Z, Chen M, Liu Z. *Adv Funct Mater*, 2016, 26: 2207–2217

20 Bhaskaran V, Nowicki MO, Idriss M, Jimenez MA, Lugli G, Hayes JL, Mahmoud AB, Zane RE, Passaro C, Ligon KL, Haas-Kogan D, Bronisz A, Godlewski J, Lawler SE, Chiocca EA, Peruzzi P. *Nat Commun*, 2019, 10: 442

21 Zarredar H, Pashapour S, Ansarin K, Khalili M, Baghban R, Farajnia S. *J Cell Physiol*, 2019, 234: 1560–1566

22 Zhu N, Weng S, Wang J, Chen J, Yu L, Fang X, Yuan Y. *J Cancer Res Clin Oncol*, 2019, 145: 3021–3036

23 Housman G, Byler S, Heerboth S, Lapinska K, Longacre M, Snyder N, Sarkar S. *Cancers*, 2014, 6: 1769–1792

24 Wu J, Zhao L, Xu X, Bertrand N, Choi WI, Yameen B, Shi J, Shah V, Mulvale M, MacLean JL, Farokhzad OC. *Angew Chem Int Ed*, 2015, 54: 9218–9223

25 Zheng M, Ruan S, Liu S, Sun T, Qu D, Zhao H, Xie Z, Gao H, Jing X, Sun Z. *ACS Nano*, 2015, 9: 11455–11461

26 Zhu G, Mei L, Vishwasrao HD, Jacobson O, Wang Z, Liu Y, Yung BC, Fu X, Jin A, Niu G, Wang Q, Zhang F, Shroff H, Chen X. *Nat Commun*, 2017, 8: 1482

27 Zhang L, Abdullah R, Hu X, Bai H, Fan H, He L, Liang H, Zou J, Liu Y, Sun Y, Zhang X, Tan W. *J Am Chem Soc*, 2019, 141: 4282–4290

28 Guo Y, Li S, Wang Y, Zhang S. *Anal Chem*, 2017, 89: 2267–2274

29 Lee JB, Hong J, Bonner DK, Poon Z, Hammond PT. *Nat Mater*, 2012, 11: 316–322

30 Bai J, Jia X, Zhen W, Cheng W, Jiang X. *J Am Chem Soc*, 2018, 140: 106–109

31 Johnson CD, Esquela-Kerscher A, Stefani G, Byrom M, Kelnar K, Ovcharenko D, Wilson M, Wang X, Shelton J, Shingara J, Chin L, Brown D, Slack FJ. *Cancer Res*, 2007, 67: 7713–7722

32 Mou J, Lin T, Huang F, Chen H, Shi J. *Biomaterials*, 2016, 84: 13–24

33 Deng X, Cao M, Zhang J, Hu K, Yin Z, Zhou Z, Xiao X, Yang Y, Sheng W, Wu Y, Zeng Y. *Biomaterials*, 2014, 35: 4333–4344

34 Huang L, Tao K, Liu J, Qi C, Xu L, Chang P, Gao J, Shuai X, Wang G, Wang Z, Wang L. *ACS Appl Mater Interfaces*, 2016, 8: 6577–6585

35 Ren K, Liu Y, Wu J, Zhang Y, Zhu J, Yang M, Ju H. *Nat Commun*, 2016, 7: 13580

36 Chen Z, Zeng H, Guo Y, Liu P, Pan H, Deng A, Hu J. *J Exp Clin Cancer Res*, 2010, 29: 151

37 Kulkarni A, Natarajan SK, Chandrasekar V, Pandey PR, Sengupta S. *ACS Nano*, 2016, 10: 9227–9242

38 Kim M, Mun H, Sung CO, Cho EJ, Jeon HJ, Chun SM, Jung DJ, Shin TH, Jeong GS, Kim DK, Choi EK, Jeong SY, Taylor AM, Jain S, Meyerson M, Jang SJ. *Nat Commun*, 2019, 10: 3991

39 Jang M, Kim JH, Nam HY, Kwon IC, Ahn HJ. *Nat Commun*, 2015, 6: 7930

40 Bagalkot V, Farokhzad OC, Langer R, Jon S. *Angew Chem Int Ed*, 2010, 45: 8149–8152

41 Daly TA, Wang M, Regen SL. *Langmuir*, 2011, 27: 2159–2161

42 Shiao YS, Chiu HH, Wu PH, Huang YF. *ACS Appl Mater Interfaces*, 2014, 6: 21832–21841

43 Wu Y, Zhang H, Xiang J, Mao Z, Shen G, Yang F, Liu Y, Wang W, Du N, Zhang J, Tang Y. *Talanta*, 2018, 179: 501–506